Molecular Simulation, Vol. 32, No. 6, 15 May 2006, 465–470

Taylor & Francis
Taylor & Francis Group

Pressure and thermal effects on elastic properties of single crystal α-Al_2O_3 from Monte-Carlo simulation

Z.-B. WU†* and Q.-J. XING‡

†State Key Laboratory of Nonlinear Mechanics, Institute of Mechanics, Chinese Academy of Sciences, Beijing 100080, China
‡Department of Physics, Peking University, Beijing 100871, China

(Received December 2005; in final form February 2006)

A rectangular structural unit cell of α-Al_2O_3 is generated from its hexagonal one. For the rectangular structural crystal with a simple interatomic potential [Matsui, *Mineral Mag.* **58A**, 571 (1994)], the relations of lattice constants to homogeneous pressure and temperature are calculated by using Monte-Carlo method at temperature 298 K and 0 GPa, respectively. Both numerical results agree with experimental ones fairly well. By comparing pair distribution function, the crystal structure of α-Al_2O_3 has no phase transition in the range of systematic parameters. Based on the potential model, pressure dependence of isothermal bulk moduli is predicted. Under variation of general strains, which include of external and internal strains, elastic constants of α-Al_2O_3 in the different homogeneous load are determined. Along with increase of pressure, axial elastic constants increase appreciably, but nonaxial elastic constants are slowly changed.

Keywords: Alumina; Pressure dependence; Thermal effect; Monte-Carlo simulation

1. Introduction

Sapphire or Corundum (α-Al_2O_3), as the most stable phase of alumina, has important physical and chemical properties for application: great hardness, chemical inertness and a high melting point. Indeed, corundum has been widely used as a window material in shock-wave experiments [1], as well as, coating material in wear-resistant cutting tools [2]. It is thus important to know high-pressure elastic properties of the alumina. The elastic properties of corundum, such as pressure dependence [3,4], temperature dependence [5] and high-order elastic constants [6], have been measured in experiments. However, few atomistic simulation studies on them due to limited development of its potential models. Based on the Buckingham potential and the core-shell model, elastic constants and dynamical properties of solid α-Al_2O_3 are reported [7,8]. By implying electrostatic energy to the embedded-atom method, an electrostatic potential for solid α-Al_2O_3 is suggested and applied to determine surfaces relaxation [9]. Recently, a simple potential model named as CMAS94 is proposed by combining the Buckingham potential and Ewald summation of Coulomb interaction [10,11]. It can be applied to describe the structural properties of solid and liquid α-Al_2O_3 [10–13].

In this paper, a rectangular structural unit cell of single crystal α-Al_2O_3 is proposed. Based on the CMAS94 potential model, structural parameters in relations to pressure and temperature are determined by using Monte-Carlo method and compared with experimental results. Pressure dependence of isothermal bulk moduli and elastic constants are predicted.

2. Crystallography, model and method

The crystallographic specification of α-Al_2O_3 belongs to the space group $R\bar{3}c$ and its crystallography is rhombohedral. It is commonly described in the hexagonal structural unit cell with $a = 4.759$ Å and $c = 12.991$ Å [14]. The unit cell with 30 atoms (12 Al and 18 O) embedded in body coordinates is generated by using the procedure described in [15]. After transformation from body coordinates (ξ,η,ζ) to Cartesian coordinates (x,y,z) by using

$$x = \frac{\sqrt{3}}{2}a\xi, \quad y = a\eta - \frac{1}{2}a\xi, \quad z = c\zeta, \tag{1}$$

*Corresponding author. Email: wuzb@lnm.imech.ac.cn

Molecular Simulation
ISSN 0892-7022 print/ISSN 1029-0435 online © 2006 Taylor & Francis
http://www.tandf.co.uk/journals
DOI: 10.1080/08927020600789151

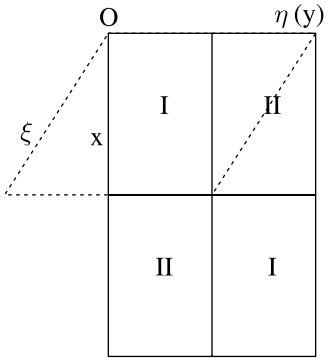

Figure 1. A plane schematic for combining two hexagonal unit cells to a rectangular one through transformation of the body coordinates (ξ, η, ζ) to Cartesian coordinates (x, y, z). Dot and solid lines denote the hexagonal and the rectangular unit cells, respectively.

we cut and paste a triangular prism, so that the rhombic prism is changed to a cuboid, which has only periodic conditions in y and z directions. In x direction, two half sides (I and II) are interlaced with another ones. In order to keep the periodic condition in x direction, we add another cuboid in the direction. The order of two half bodies (I and II) of the cuboid is exchanged in y direction. Thus, two hexagonal structural unit cells (rhombic prisms) are divided and combined as a rectangular one in figure 1. The three-dimensional crystal structure with 60 atoms (24 Al and 36 O) is drawn in figure 2. It preserves the periodic boundary condition of crystal structure and has crystal lengths of $l_x = a$, $l_y = \sqrt{3}a$ and $l_z = c$. Since the transformation from hexagonal structural unit cells to the rectangular one is reversible, the lattice parameters in both unit cells are correspondent.

In the CMSA94 model, the configurational (potential) energy U is expressed as a sum of two-body potentials

$$U = U_p + U_e = \frac{1}{2}\sum_{i=1}^{N}\sum_{j\neq i}^{N}\left[\phi_p(r_{ij}) + \frac{q_i q_j}{4\pi\varepsilon_0 r_{ij}}\right], \qquad (2)$$

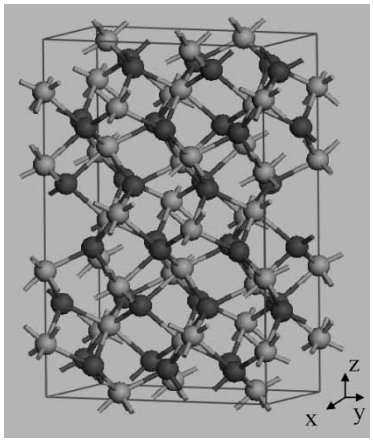

Figure 2. Schematic of the α-Al_2O_3 rectangular structural unit cell. Light and dark circles denote the ions Al^{+3} and O^{-2}, respectively.

Table 1. Configurational energy parameters in the simulation.

	$q(\lvert e\rvert)$	$a(\text{Å})$	$b(\text{Å})$	$c[\text{Å}^3(kJ/mol)^{1/2}]$
Al	1.4175	0.7852	0.034	36.82
O	−0.945	1.8215	0.138	90.61

where

$$\phi_p(r_{ij}) = -\frac{c_i c_j}{r_{ij}^6} + f(b_i + b_j)\exp\left[\frac{a_i + a_j - r_{ij}}{b_i + b_j}\right]. \qquad (3)$$

Its terms represent van der Waals repulsion and Coulomb interactions, respectively. Here, r_{ij} is the interatomic distance between a pair of atoms i and j, f is a standard force constant of $4.184\,\text{kJ}\,\text{Å}^{-1}\,\text{mol}^{-1}$. The net charge q_i, repulsive radii a_i, softness parameters b_i and van der Waals coefficients c_i of the ion i are listed in table 1. Monte-Carlo simulations are worked in the isothermal-isobaric ensemble (NPT) for a rectangular structural cell with $N = 2160$ atoms (864 Al and 1296 O). The cell box has 36 rectangular structural unit cells. Its lengths are $L_x = 6l_x = 28.554\,\text{Å}$, $L_y = 3l_y = 24.728\,\text{Å}$ and $L_z = 2l_z = 25.982\,\text{Å}$. We evaluate the short-range terms using direct summation under periodic boundary conditions. The cutoff radius r_c is taken as a half of the minimal box length. The long-range coulomb term is treated by using standard Ewald techniques as following [16,17]

$$\begin{aligned} 4\pi\varepsilon_0 U_e &= 4\pi\varepsilon_0(U_r + U_k + U_c) \\ &= \frac{1}{2}\sum_{i=1}^{N}\sum_{j=1}^{N} q_i q_j \sum\nolimits'^{\infty}_{|\mathbf{n}|=0} \phi_r(R_{ij}) \\ &+ \frac{1}{2\pi V}\sum_{\mathbf{m}\neq 0}\frac{\exp^{-\pi^2 k_m^2/\kappa^2}}{k_m^2} S(\mathbf{k_m})S(-\mathbf{k_m}) \\ &- \frac{\kappa}{\pi^{1/2}}\sum_{i=1}^{N} q_i^2, \end{aligned} \qquad (4)$$

where

$$\begin{aligned} \phi_r(R_{ij}) &= \frac{\text{erfc}(\kappa R_{ij})}{R_{ij}}, \\ S(\mathbf{k_m}) &= \sum_{i=1}^{N} q_i \exp(2\pi i \mathbf{k_m}\cdot\mathbf{r_i}) \end{aligned} \qquad (5)$$

and $\mathbf{R}_{ij} = \mathbf{r}_{ij} + [\mathbf{h}]\mathbf{n}$, $R_{ij} = |\mathbf{R}_{ij}|$ and $\mathbf{k_m} = [\mathbf{h}]^{-1}\mathbf{m}$, $k_m = |\mathbf{k_m}|$. $[\mathbf{h}]$ is a 3×3 diagonal matrix with main diagonal elements L_x, L_y and L_z. V is a volume of the rectangular structural crystal. In the Ewald method, the contribution of the summation between real- and reciprocal-space is controlled by a parameter κ, which is weighted as $\kappa = (N\pi^3/V^2)^{1/3}$ [18].

From classical Helmholtz free energy, using the macroscopic Lagrangian strain [19] $\varepsilon_{\alpha\beta} = (1/2)(u_{\alpha\beta} + u_{\beta\alpha} + \sum_{\gamma=1}^{3} u_{\gamma\alpha}u_{\gamma\beta})$, the systematic stress tensor $\tau_{\alpha\beta}$ can

be expressed as

$$\tau_{\alpha\beta} = -\frac{Nk_{\mathrm{B}}T}{V}\delta_{\alpha\beta} + \frac{1}{2}\sum_{i=1}^{N}\sum_{j\neq i}^{N} \left[\frac{6c_ic_j}{r_{ij}^7} - f\exp\left(\frac{a_i + a_j - r_{ij}}{b_i + b_j}\right)\right]\frac{r_{ij\alpha}r_{ij\beta}}{r_{ij}} + \frac{1}{2}\sum_{i=1}^{N}\sum_{j=1}^{N} q_iq_j{\sum_{|\mathbf{n}|}}' \left[-\frac{2\kappa}{\sqrt{\pi}R_{ij}}\exp(-\kappa^2R_{ij}^2) - \frac{\mathrm{erfc}(\kappa R_{ij})}{R_{ij}^2}\right] \times\frac{R_{ij\alpha}R_{ij\beta}}{R_{ij}} + \frac{1}{2\pi V}\sum_{\mathbf{m}\neq 0}\frac{\mathrm{e}^{-\pi^2k_m^2/\kappa^2}}{k_m^2} \left[\left(1 + \frac{\pi^2k_m^2}{\kappa^2}\right)\frac{2k_{m\alpha}k_{m\beta}}{k_m^2} - \delta_{\alpha\beta}\right]S(\mathbf{k_m})S(-\mathbf{k_m}), \tag{6}$$

where δ is the Kronecker symbol, k_{B} is Boltzmann's constant and $\alpha,\beta \in \{x,y,z\}$.

In the NPT Monte-Carlo simulation [16], the Markov chain is generated using Metropolis algorithm. Two kinds of trial moves in each cycle are necessary to explore the configuration space of the system: translations of the ion centers of mass and changes of the size of the rectangular cell. In special, we independently change L_x and L_z and keep the relation $L_y = \sqrt{3}L_x/2$. A trial move from the state m to n is accepted with a probability equal to $\min[\exp(-\beta\delta H_{nm}), 1]$, where $\delta H_{nm} = \delta U_{nm} + P(U_n - U_m) - N\beta^{-1}\ln(U_n/U_m)$. We throw away a half of $M(= 1000)$ cycles and calculate ensemble averages in the last half of M. Using the Monte-Carlo simulation, we can arrive at an equilibrium state of system under a homogeneous load.

3. Results and discussions

3.1 Pressure and thermal effects on structures

We perform the NPT Monte-Carlo method to investigate pressure and thermal effects on structures. The configurational energy is given by equation (2). Six independent stresses are calculated by equation (6) to confirm the homogeneous load in each simulation. Since the load on the rectangular cell is homogeneous, three shear stresses always keep zero and only three normal stresses are taken for confirmation.

Firstly, the systematic temperature is fixed at 298 K and P is constrained as different values. We calculate the ensemble average of rectangular cell lengths and transfer to $< a >$ and $< c >$ of hexagonal structural unit cell. The results are drawn in figure 3(a) and (b). Along with the increase of P, both $< a >$ and $< c >$ monotonically decrease. To compare with experimental measurement values, we also plot corresponding experimental data [3,4], where the fluctuations for average values of a and c are ± 0.02 and ± 0.10 Å, respectively. The standard derivations (percent errors) of a and c between numerical and experimental values are about 0.06 Å(1.3%) and 0.11 Å(0.8%), respectively. Our numerical results agree with the experimental ones fairly well.

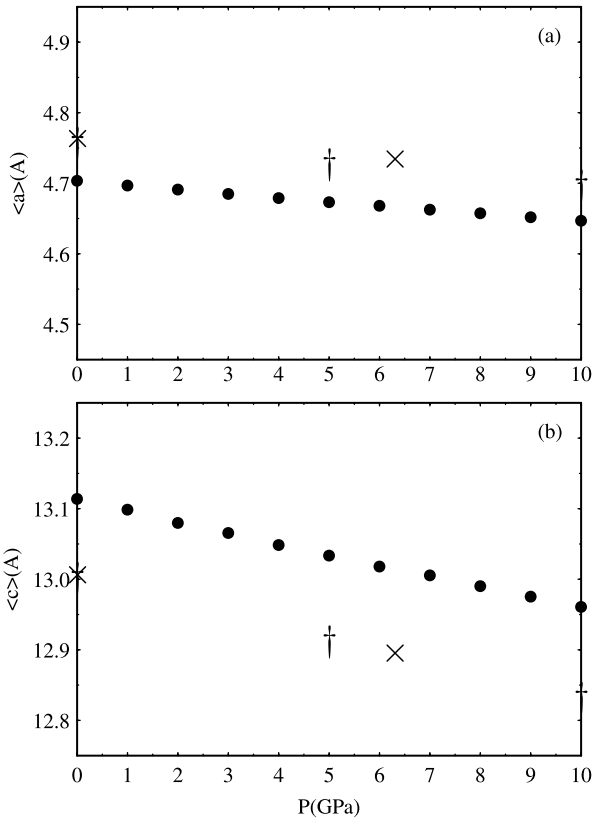

Figure 3. Lattice lengths of α-Al_2O_3 hexagonal structural unit cell vs homogeneous pressure at $T = 298$ K: (a) $< a >$, (b) $< c >$. Dots, crosses and dags denote the current results, experimental results of [3] and [4], respectively.

In order to analyze the evolution of crystal structure of $\alpha - Al_2O_3$ under pressure, we plot correspondent pair distribution function $g(r)$ in figure 4. It is found that the function $g(r)$ is almost independent of the increase of pressure. The distribution of peaks does not change, but their relative positions have a global move under pressure.

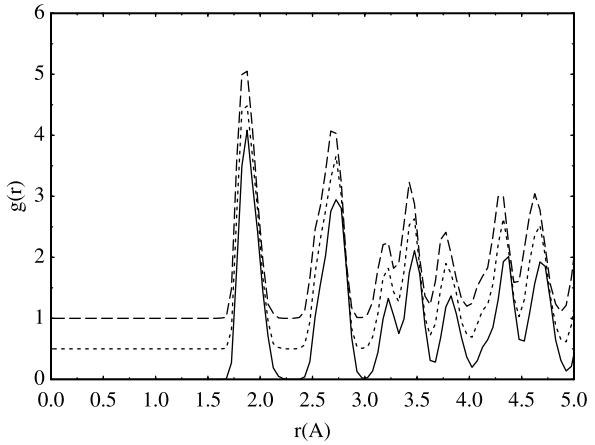

Figure 4. Pair distribution function of α-Al_2O_3 at $T = 298$T and different hydrostatic pressure P. Solid, dot and dash lines denote $P = 0$ GPa $[g(r)]$, 5 GPa $[g(r) + 0.5]$ and 10 GPa $[g(r) + 1.0]$, respectively.

In the process, only the crystal size and relative positions of ions are compressed, so the single crystal $\alpha-Al_2O_3$ is kept as the same phase.

Then, the systematic homogeneous pressure is constrained as 0 GPa in the change of *T*. The ensemble averages $< a >$ and $< c >$ of hexagonal structural unit cell vs the temperature are plotted in figure 5(a) and (b). Along with the increase of *T*, both $< a >$ and $< c >$ monotonically increase. To compare with experimental results, we also draw correspondent experimental data [20]. The standard derivations (percent errors) of *a* and *c* between numerical and experimental values are about 0.05 Å(1.1%) and 0.15 Å(1.2%), respectively. Our numerical results with small percent errors keep an agreement with the experimental ones.

Figure 6 displays the pair distribution function $g(r)$ in different temperature. Along with the increase of temperature, $g(r)$ decreases, but relative positions of the peaks are independent. In the process, although the crystal size is blown up, the relative position of ions, i.e. the structure of crystal does not change. So the single crystal $\alpha - Al_2O_3$ is kept as the same phase.

So far, the CMAS94 model has been validated in the ranges of hydrostatic pressure and temperature. By comparing pair distribution function, the α phase of Al_2O_3 is kept during the process. In the following, using the model, we will predict elastic properties of α-Al_2O_3 under pressure.

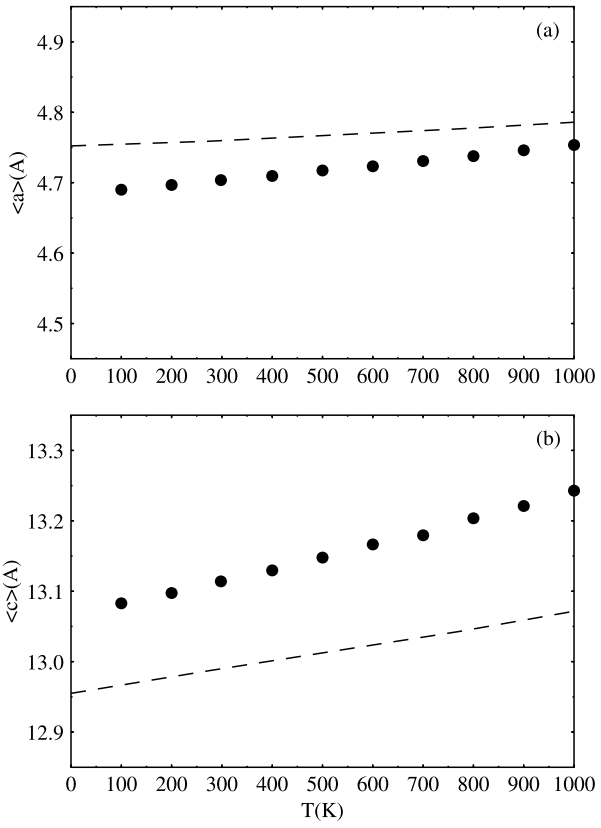

Figure 5. Lattice lengths of α-Al_2O_3 hexagonal structural unit cell vs temperature at $P = 0$ GPa: (a) $< a >$, (b) $< c >$. Dots and line denote the current results and fitting of experimental results of [20], respectively.

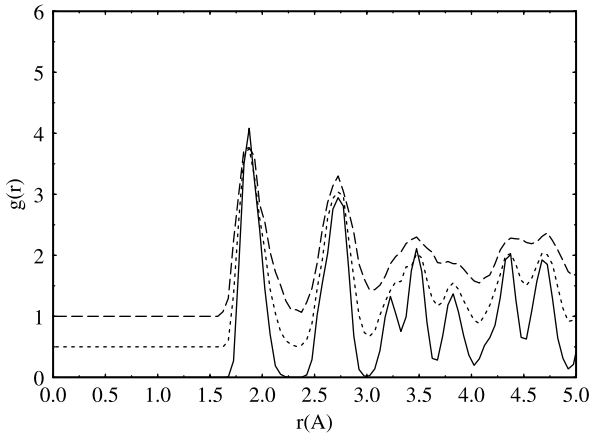

Figure 6. Pair distribution function of α-Al_2O_3 at $P = 0$ GPa and different temperature *T*. Solid, dot and dish lines denote $T = 298$ K $[g(r)]$, 600 K $[g(r) + 0.5]$ and 1000 K $[g(r) + 1.0]$, respectively.

3.2 Pressure dependence of isothermal bulk moduli

To describe volume comprehensibility of α-Al_2O_3, we calculate the proportional decrease in volume of a crystal when subjected to hydrostatic pressure. The isothermal bulk moduli *K* of a crystal is expressed as

$$K = -V\left(\frac{\partial P}{\partial V}\right)_T. \tag{7}$$

The systematic temperature is fixed at 298 K. The hydrostatic pressure is changed in the range of 0–10 GPa. Under each pressure, *P* varying in ± 0.2 and ± 0.5 GPa, using the NPT Monte-Carlo method, we calculate correspondent volumes. The data approaches to a global continues function of the pressure. Using the 6-order polynomial least-squares refinement method to fit the relation of volume to pressure, we obtain the following equation

$$\begin{aligned} V(P) = {} & 17749.1 - 63.1(P - 5.0) \\ & + 7.6 \times 10^{-1}(P - 5.0)^2 - 1.0 \times 10^{-2}(P - 5.0)^3 \\ & - 4.6 \times 10^{-4}(P - 5.0)^4 - 2.2 \times 10^{-4}(P - 5.0)^5, \end{aligned} \tag{8}$$

where the dimensions of *P* and *V* are GPa and $Å^3$, respectively. In order to compare with experimental result, from equations (7) and (8), we determine the isothermal bulk moduli $K = 251.4$ GPa at $P = 0$ GPa. The experimental isothermal bulk moduli [5] for $P = 0$ GPa and $T = 296$ K is $K = 252.3$ GPa. So the numerical simulation result is very close to the experimental measurement value.

In order to display the effect of pressure on isothermal bulk moduli, from equations (6) and (7), we calculate *K* at different hydrostatic pressure *P* and draw results in figure 7. Along with the increase of *P*, *K* monotonically increases. This behavior correspondents to the compressibility of crystal size without any changes of crystal structure under pressure.

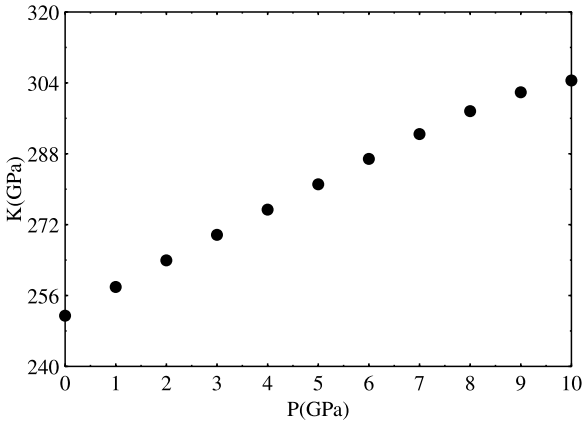

Figure 7. Isothermal bulk moduli K of α-Al_2O_3 vs homogeneous pressure P at $T = 298$ K.

3.3 Pressure dependence of elastic constants

The crystal structure of α-Al_2O_3 has not a central symmetry, so its general strains include of six external strains $u_{\alpha,\beta}$ and $3N$ internal strains $r_{i\xi}$. Under an assumption of small strains $u_{\alpha,\beta}$ can be transferred as the macroscopic Lagrangian strain $\varepsilon_{\alpha\beta}$. To calculate the elastic constants, following the derivation at zero Kelvin [19,21], we obtain the second-order elastic constants for $\alpha - Al_2O_3$:

$$[C] = \frac{1}{V}\left\{\left[\frac{\partial^2 U}{\partial\varepsilon_{\alpha\beta}\partial\varepsilon_{\mu\nu}}\right] - \left[\frac{\partial^2 U}{\partial\varepsilon_{\alpha\beta}\partial r_{i\xi}}\right]\left[\frac{\partial^2 U}{\partial r_{i\xi}\partial r_{j\eta}}\right]^{-1}\left[\frac{\partial^2 U}{\partial r_{j\eta}\partial\varepsilon_{\mu\nu}}\right]\right\}, \tag{9}$$

where $\mu, \nu, \xi, \eta \in \{x, y, z\}$, i and j are indices of atoms.

To check the generated rectangular structural unit cell and the formula of elastic constants, we make a comparison with the GULP software [22]. The hexagonal structural parameters from the experimental data [14] are chosen as initial ones in GULP and optimized to get structural parameters at zero pressure and zero Kelvin: $a = 4.683$ Å, $c = 13.066$ Å, $z_{Al} = 0.348$ and $x_O = 0.315$. By using the above method a rectangular structural cell with 2160 atoms is generated. Using equation (9), we calculate elastic constants and display results in table 2, where results obtained by GULP are also included. Since the space group of α-Al_2O_3 is $R\bar{3}c$, only six independent elastic constants are given. Both results are almost the same. To check the elastic constants predicted by the CMSA94 potential model, we present experimental results [6,23] in table 2. Except C_{13}, C_{14} and C_{44}, the calculated results are close to the experimental results. The axial elastic constants are more exactly predicted than the nonaxial ones. As reported in [10,11], the configurational energy parameters in table 1 can reproduce the observed structural data and isothermal bulk moduli of alumina as accurately as possible. Thus, to exactly estimate the elastic constants of alumina, the configurational energy parameters will be renewed. However, if we accept the absolute errors of ± 40 GPa of elastic constants in realistic application, the calculated results compare fairly well with the experimental ones.

To calculate the elastic constants of alumina as a function of external homogeneous pressure, we assume that the lattice constants of α-Al_2O_3 are nearly the same for $T = 100$ and 0 K. This assumption appears to be reasonable as the melting temperature of corundum is above two thousands Kelvin. With this assumption, we employ the averaged lattice constants calculated at various external pressures from the NPT Monte-Carlo simulation as the input lattice parameters in formula (9). Note that formula (9) is derived for crystals at $T = 0$ K. To examine this assumption, we calculate the "zero-temperature and zero-pressure" elastic constants based on the lattice structure obtained at $T = 100$ K. The results, marked by $T = 0^*(100)$ K in table 2, are close to the above realistic zero-temperature and zero-pressure elastic constants.

Figure 8 displays plots of the elastic constants vs homogeneous pressure. Along with increase of pressure, C_{11} and C_{33} increase appreciably, C_{12}, C_{13} and C_{44} only increase slightly and C_{14} is nearly unchanged. To compare pressure derivatives of the elastic constants at zero pressure, we present our calculating results and experimental data [4,6] in table 3, where the calculated results are estimated from a numerical linear interpolation at three different pressures, -0.5, 0 and 0.5 GPa. The calculated and experimental results agree reasonably well.

4. Conclusion

In summary, a rectangular structural unit cell of α-Al_2O_3 is generated from its hexagonal one. For the rectangular structural crystal, the relations of lattice constants to homogeneous pressure and temperature are calculated by using Monte-Carlo method. The numerical results with small percent errors agree with the experimental measurement values. By analyzing the pair distribution function, the crystal structure of α-Al_2O_3 has no phase

Table 2. Elastic constants of α-Al_2O_3 at zero pressure.

	T (K)	C_{11} (GPa)	C_{12} (GPa)	C_{13} (GPa)	C_{33} (GPa)	C_{14} (GPa)	C_{44}(GPa)
Present work	0	478.0	183.1	151.9	524.9	18.7	117.1
GULP [21]	0	478.0	183.1	151.9	524.3	18.7	117.1
Present work	0* (100)	457.9	176.8	141.2	507.2	19.3	110.5
Ref. [6]	297	495.4	162.1	109.2	496.5	−23.5	147.4
Ref. [22]	298	496.8	163.6	110.9	498.1	−23.5	147.4

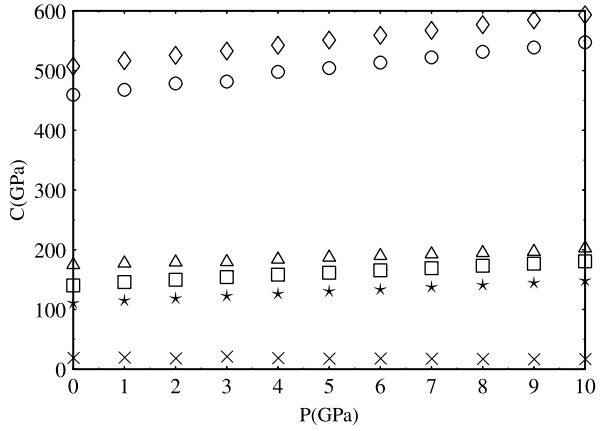

Figure 8. Elastic constants of α-Al_2O_3 vs a homogeneous pressure *P*. C_{11}, C_{12}, C_{13}, C_{33}, C_{14} and C_{44} are marked by circles, triangles, squares, diamonds, crosses and stars, respectively.

Table 3. Pressure derivatives of elastic constants of α-Al_2O_3 at zero pressure.

	T (K)	$\frac{dC_{11}}{dP}$	$\frac{dC_{12}}{dP}$	$\frac{dC_{13}}{dP}$	$\frac{dC_{33}}{dP}$	$\frac{dC_{14}}{dP}$	$\frac{dC_{44}}{dP}$
Present work	0* (100)	8.7	3.9	4.2	8.7	0.7	2.5
Ref. [4]	298	6.2	3.3	3.6	4.9	0.1	2.2
Ref. [6]	297	6.2	3.3	3.8	5.3	0.2	2.3

transition in the range of systematic parameters. Based on the CMAS94 potential model, pressure dependence of isothermal bulk moduli is predicted. At a given pressure, for isothermal bulk moduli, the numerical result has a good agreement with the experimental one. Under variation of general strains, which include of external and internal strains, elastic constants of α-Al_2O_3 in the different homogeneous load are determined. Along with increase of pressure, axial elastic constants increase appreciably, but nonaxial elastic constants are slowly changed.

To the best of our knowledge, pressure dependence of isothermal bulk moduli and elastic constants of α-Al_2O_3 have not been reported in the literatures. Based on the CMAS94 potential model, we predicate the pressure dependence of isothermal bulk moduli and elastic constants.

Acknowledgements

We thank the Chinese Academy of Sciences (KJCX2-SW-L2) and the K. C. Wong Education Foundation of Hong Kong. We also thank LSEC and ICTS research computing facilities for assisting us in the computation.

References

[1] C.S. Yoo, N.C. Homes, E. See. In *Shock Compression of Condensed Matter—1991*, S. Schmidt, R.D. Dick, J.W. Forbes, D.G. Pasker (Eds.), Amsterdam, North-Holland (1992).
[2] P. Hansson, M. Halvarsson, S. Vuorinen. Characterization of the k-Al_2O_3-α-Al_2O_3 transformation in different single layer coatings of CVD k-Al_2O_3. *Surf. Coat. Technol.*, **76–77**, 256 (1995).
[3] H.V. Hart, H.G. Drickamer. Effect of high pressure on the lattice parameters of Al_2O_3. *J. Chem. Phys.*, **43**, 2265 (1965).
[4] J.H. Gieske, G.R. Barsch. Pressure dependence of the elastic constants of single crystalline aluminum oxide. *Phys. Status Solidi*, **29**, 121 (1968).
[5] T. Goto, O.L. Anderson, I. Ohno, S. Yamamoto. Elastic constants of Corundum up to 1825 K. *J. Geophys. Res.*, **94**, 7588 (1989).
[6] R.E. Hankey, D.E. Schuele. Third-order elastic constants of Al_2O_3. *J. Acoust. Soc. Am.*, **48**, 190 (1970).
[7] C.R.A. Catlow, R. James, W.C. Mackrodt, R.F. Stewart. Defect energetics in α-Al_2O_3 and rutile TiO_2. *Phys. Rev. B*, **25**, 1006 (1982).
[8] C. Rambaut, H. Jobic, H. Jaffrezic, J. Kohanoff, S. Fayeulle. Molecular dynamics simulation of the α-Al_2O_3 lattice: dynamical properties. *J. Phys.: Cond. Matt.*, **10**, 4221 (1998).
[9] F.H. Streitz, J.W. Mitmire. Electrostatic potentials for metal-oxide surfaces and interfaces. *Phys. Rev. B*, 11996 (1994).
[10] M. Matsui. A transferable interatomic potential model for crystals and melts in the system CaO-MgO-Al_2O_3–SiO_2. *Mineral Mag.*, **58A**, 571 (1994).
[11] M. Matsui. Molecular dynamics study of the structures and bulk moduli of crystals in the system CaO-MgO-Al_2O_3–SiO_2. *Phys. Chem. Minerals*, **23**, 345 (1996).
[12] G. Gutiérrez, A.B. Belonoshko, R. Ahuja, B. Jöhansson. Structural properties of liquid Al_2O_3: a molecular dynamics study. *Phys. Rev. E*, **61**, 2723 (2000).
[13] G. Gutiérrez, B. Jöhansson. Molecular dynamics study of structural properties of amorphous Al_2O_3. *Phys. Rev. B*, **65**, 104202 (2002).
[14] W.E. Lee, K.P.D. Lagerlof. Structural and electron diffraction data for sapphire (α-Al_2O_3). *J. Elect. Micro. Tech.*, **2**, 247 (1985).
[15] H.D. Megaw. *Crystal Structure: A Working Approach*, W.B. Saunders, Philadelphia (1973), Chap. 11.
[16] M.P. Allen, D.J. Tildesley. *Computer Simulation of Liquids*, Clarendon Press, Oxford (1989), Chap. 5.
[17] S. Nosé, M.L. Klein. Constant pressure dynamics for molecular systems. *Mol. Phys.*, **50**, 1055 (1983).
[18] R.A. Jackson, C.R.A. Catlow. Computer simulation studies of zeolite structure. *Mol. Simul.*, **1**, 207 (1988).
[19] M. Born, K. Huang. *Dynamical Theory of Crystal Lattices*, Clarendon Press, Oxford (1954), Chap. III.
[20] P. Aldebert, J.P. Traverse. Neutron diffraction study of structural characteristics and ionic mobility of α-Al_2O_3 at high temperatures. *J. Am. Ceram. Soc.*, **65**, 460 (1982).
[21] C.R.A. Catlow, W.C. Mackrodt. *Computer Simulation of Solids*, Lecture Notes in Physics no. 166, Springer-Verlag, Berlin (1982), Chap. 1.
[22] J.D. Gale. *General Utility Lattice Program (GULP)*, Department of Chemistry, Imperial College, London version 1.2 (2003).
[23] J.B. Wachtman Jr., W.E. Tefft, D.G. Lam Jr., R.P. Stinchfield. Elastic constants of synthetic single crystal corundum at room temperature. *J. Res. Natl. Bur. Stand.*, **64A**, 213 (1960).